Effect of a Simple Storm on a Simple Ocean

Jeff Moehlis

1 Introduction: Near-Inertial Oscillations and Storms

Horizontal motion of a free particle on the Earth's surface subject only to the Coriolis force is governed by the equations

$$\frac{du_p}{dt} - fv_p = 0, \qquad \frac{dv_p}{dt} + fu_p = 0,$$

where u_p and v_p are respectively the eastward and northward components of the particle's velocity in the frame rotating with the Earth, $f \equiv 2\Omega_E \sin\phi$ is the Coriolis parameter, Ω_E is the frequency of the Earth's rotation, and ϕ is the latitude (see, e.g., [4]). This has solution $u_p + iv_p = e^{-ift}(u_0 + iv_0)$, where u_0 and v_0 are the initial components of the velocity. This corresponds to the particle's velocity describing a circle of radius $(u_0^2+v_0^2)^{1/2}/f$ with frequency f. In the northern hemisphere, $f > 0$ and the particle rotates in a clockwise direction when viewed from above. The inertial frequency f is the low-frequency cutoff for internal waves in the ocean. An internal wave with frequency near f is called a near-inertial oscillation (NIO). About half of the total kinetic energy associated with internal waves in the ocean is contained in NIOs [5].

There is much observational evidence, starting with [17, 14], that wind from storms can excite near-inertial currents in the mixed layer of the ocean; recent observations include [8, 13, 15]. Simple models which treat the mixed layer as a solid slab have been quite successful at explaining the process by which wind generates such currents (see, e.g., [14, 5]). These currents decay away after the storm passes, with possible mechanisms for the decay including nonlinear interactions which transfer energy to other frequencies [12], turbulent dissipation [11], and the radiation of downward propagating NIOs excited by inertial pumping into the interior of the ocean [10]. The last mechanism will be the focus of this paper. Such downward propagation of NIOs is believed to be a significant mechanism for mixing in the upper ocean.

Observations give a time scale for the decay of the energy deposited by the passing storm on the order of ten to twenty days [8, 13, 15]. This time scale is in contrast with estimates such as that by [10] that near-inertial currents decaying through the downward propagation of NIOs and with a horizontal length scale typical of the atmospheric forcing mechanism can remain in the mixed layer for longer than a year. To account for this difference, several mechanisms for the enhancement of vertical propagation of NIOs have been suggested (these are nicely summarized in [16]), including smaller-scale fluctuations within the storms, the β effect [6], and interaction with background geostrophic or quasigeostrophic flow (see, e.g., [2, 3, 16]).

This paper considers the vertical propagation of near-inertial energy and shear deposited into the mixed layer by a storm in the presence of the β effect. The analysis uses the formalism of [18] which is briefly discussed in Section 2. In Section 3, a simplified model with three main assumptions is outlined. First, the background flow is assumed to be independent of longitude and the associated vorticity is assumed to be zero. Second, the buoyancy frequency is taken to be approximately zero in the mixed layer, and constant in the interior (i.e., beneath the mixed layer). Third, it is assumed that the storm has moved very rapidly across the ocean and has created a horizontally uniform near-inertial current to the east concentrated within the mixed layer. Section 4 uses the fact that the depth of the ocean is very much larger than the mixed layer depth to formulate and solve the model for an ocean which is (effectively) infinitely deep. Section 5 discusses the results and suggests directions for further investigation.

2 Formalism

Consider the ocean to be infinite in horizontal extent and of depth D, with the mixed layer being the portion of the ocean with $-H_{\rm mix} < z < 0$, and the interior the portion with $-D < z < -H_{\rm mix}$. The x and y axes are taken to point to the east and north, respectively. The buoyancy frequency $N = N(z)$ is an arbitrary piecewise continuous function of depth z.

2.1 Evolution Equation

Young and Ben Jelloul [18] derive an evolution equation for a complex field $A(x, y, z, t)$ from which leading-order NIO motion in the presence of a steady barotropic background flow and the β effect can be deduced:

$$LA_t + \frac{\partial(\psi, LA)}{\partial(x,y)} + \frac{i}{2} f_0 \nabla^2 A + i\left(\beta y + \frac{1}{2}\zeta\right) LA = 0, \tag{1}$$

where

$$LA = \frac{\partial}{\partial z}\left(\frac{f_0^2}{N^2}\frac{\partial A}{\partial z}\right), \tag{2}$$

ψ is the streamfunction for the background flow, $\zeta \equiv \nabla^2\psi$ is the associated vorticity, and the Coriolis parameter $f = f_0 + \beta y$. Here ∇ is the horizontal gradient, and $\nabla^2 = \partial_x^2 + \partial_y^2$. Subscripts denote partial differentiation. The asymptotic expansion used in the derivation of equation (1) relies upon the frequency of near-inertial waves being close to the inertial frequency f_0. The NIO velocity field (u, v, w), buoyancy b, and pressure p are given by

$$\begin{aligned} u + iv &= e^{-if_0 t} LA \\ w &= -\frac{1}{2} f_0^2 N^{-2} (A_{xz} - iA_{yz}) e^{-if_0 t} + c.c. \\ b &= \frac{i}{2} f_0 (A_{xz} - iA_{yz}) e^{-if_0 t} + c.c. \\ p &= \frac{i}{2} (A_x - iA_y) e^{-if_0 t} + c.c. \end{aligned} \tag{3}$$

Here b is related to the density ρ by

$$\rho = \rho_0 \left[1 - \frac{1}{g} \int_0^z N^2(z')dz' - \frac{b}{g} \right],$$

where ρ_0 is the reference density at the top of the ocean. Note that p has been normalized by ρ_0.

The boundary conditions are that w vanishes at the top and bottom of the ocean; this corresponds to the boundary condition $A_z = 0$ at $z = 0$ and $z = -D$. This boundary condition along with equation (3) implies that

$$\int_{-D}^{0} (u + iv) = 0. \tag{4}$$

Thus, the barotropic motion is not included in the analysis; note that [10] shows that the barotropic response to a storm is instantaneous and the associated currents are weak.

2.2 Jump Conditions

Suppose that the buoyancy frequency is discontinuous at $z = z_d$. Integrating equations (2) and (3) from $z = z_d - \delta$ to $z = z_d + \delta$, the following jump condition is obtained:

$$\left[\frac{f_0^2}{N^2} \frac{\partial A}{\partial z} \right]_{z_d-\delta}^{z_d+\delta} = e^{if_0 t} \int_{z_d-\delta}^{z_d+\delta} (u + iv)dz.$$

The left hand side tends to zero as $\delta \to 0$ provided u and v remain finite (which must be true on physical grounds). Thus, $\frac{1}{N^2}\frac{\partial A}{\partial z}$ is continuous, even when N^2 is discontinuous. Now assuming that ψ and ζ have no δ-function behavior in the z direction, integrating equation (1) over the same interval in z implies that

$$\lim_{\delta \to 0} \int_{z_d-\delta}^{z_d+\delta} \nabla^2 A \, dz = 0.$$

Thus $\nabla^2 A = A_{xx} + A_{yy}$ is continuous across $z = z_d$.

2.3 Energy and Shear

The quantities

$$u^2 + v^2 = |LA|^2, \qquad u_z^2 + v_z^2 = \left| \frac{\partial}{\partial z}(LA) \right|^2 \tag{5}$$

give local measures of the horizontal kinetic energy per unit mass (hereafter HKE) contained in near-inertial motion and the associated vertical shear, respectively. Using equation (1) and its complex conjugate,

$$\begin{aligned} \frac{\partial |LA|^2}{\partial t} &= LA_t^* \, LA + LA_t \, LA^* \\ &= \frac{if_0}{2}[\nabla \cdot (LA \, \nabla A^* - LA^* \, \nabla A)] - \frac{\partial(\psi, |LA|^2)}{\partial(x, y)} \\ &\quad + \frac{if_0}{2} \left\{ \frac{\partial}{\partial z} \left[\frac{f_0^2}{N^2} (\nabla A_z^* \cdot \nabla A - \nabla A_z \cdot \nabla A^*) \right] \right\}, \end{aligned} \tag{6}$$

where the star denotes complex conjugation. In the following, it will be useful to integrate this over a volume in order to determine how the energy contained in horizontal near-inertial motion in the volume depends on the value of derivatives of A evaluated on the surface of the volume. A general equation for the evolution of the shear is not given here, but will be for the simplified model considered next.

3 A Simplified Model

To simplify the analysis, it is assumed that A and ψ do not vary in the x direction, and that $\zeta = 0$. The analysis thus keeps the β effect but neglects the effect of background barotropic vorticity. The buoyancy frequency profile is taken to be

$$\begin{aligned} N^2 &= \epsilon^2 N_0^2 \qquad -H_{\rm mix} < z < 0 \\ N^2 &= N_0^2 \qquad -D < z < -H_{\rm mix}, \end{aligned}$$

where $\epsilon \ll 1$. Finally, the storm is assumed to produce the initial condition of a horizontally uniform near-inertial current to the east concentrated within the mixed layer.

Instead of approaching this problem by projecting onto normal modes (see, e.g., [2, 10]), the problem will be formulated as an initial value problem on a semi-infinite domain corresponding to an effectively infinitely deep ocean. In order to formulate the problem properly for this limit, this section considers an ocean of finite depth. In Section 4 the solution in the limit that the depth of the interior is much greater than the mixed layer depth will be found.

3.1 Nondimensionalization

Quantities are nondimensionalized according to

$$\hat{y} = \frac{y}{Y}, \qquad \hat{z} = \frac{z}{H_{\rm mix}} + 1, \qquad \hat{t} = \Omega t, \qquad \hat{N} = \frac{N}{N_0},$$

where

$$Y \equiv \left(\frac{H_{\rm mix}^2 N_0^2}{\beta f_0} \right)^{1/3}, \qquad \Omega \equiv \left(\frac{\beta^2 H_{\rm mix}^2 N_0^2}{f_0} \right)^{1/3}.$$

Typical values $\beta \approx 10^{-11}{\rm m}^{-1}{\rm s}^{-1}$, $H_{\rm mix} \approx 100{\rm m}$, $f_0 \approx 10^{-4}{\rm s}^{-1}$, $N_0 \approx 10^{-2}{\rm s}^{-1}$ give $Y \approx 10^5{\rm m}$ and $\Omega \approx 10^{-6}{\rm s}^{-1}$. The relevant time scale is thus $1/\Omega \approx 11.5$ days. Also, with a view to specifying the initial velocity profile according to equation (3), the velocity and the field A are nondimensionalized as

$$(\hat{u}, \hat{v}) = \frac{(u, v)}{U}, \qquad \hat{A} = \frac{f_0^2}{U N_0^2 H_{\rm mix}^2} A,$$

where U is a characteristic value of the velocity. The hats will be dropped for ease of notation. With this nondimensionalization, the buoyancy frequency profile is

$$\begin{aligned} N^2 &= \epsilon^2 \qquad 0 < z < 1 \\ N^2 &= 1 \qquad -H \equiv -\frac{D}{H_{\rm mix}} + 1 < z < 0, \end{aligned}$$

and equation (1), the boundary conditions, and initial condition become

$$A_{zzt} + \frac{i}{2}N^2 A_{yy} + iyA_{zz} = 0 \tag{7}$$

$$A_z = 0 \qquad z = -H, \;\; z = 1 \tag{8}$$

$$A_{zz} = N^2 u \qquad t = 0. \tag{9}$$

The jump conditions in nondimensional form are

$$A_z|_{z=0^+} = \epsilon^2 A_z|_{z=0^-}, \qquad A_{yy}|_{z=0^+} = A_{yy}|_{z=0^-}, \tag{10}$$

where $z = 0^+$ and $z = 0^-$ are the limits as $z \to 0$ from positive and negative z values, respectively.

This nondimensionalization allows some immediate conclusions to be drawn about the propagation of NIO energy and shear downwards. Most importantly, if H_{mix} increases then the timescale $1/\Omega$ decreases. Thus, assuming that the storm causes a uniform near-inertial current throughout the whole mixed layer, energy and shear transfer will be faster for a deeper mixed layer. This confirms the results of [10], which associated the more efficient transfer with a larger projection of the initial velocity profile on the first vertical mode.

3.2 Integral Energy Relations and Energy Flux

The nondimensional local kinetic energy per unit mass is $u^2 + v^2 = |A_{zz}/N^2|^2$. The nondimensional form of equation (6), with the assumptions of the simplified model, is

$$\frac{\partial}{\partial t}\left|\frac{A_{zz}}{N^2}\right|^2 = \frac{i}{2N^2}\,\frac{\partial}{\partial y}(A_{zz}A_y^* - A_{zz}^* A_y) + \frac{i}{2N^2}\,\frac{\partial}{\partial z}(A_{yz}^* A_y - A_{yz}A_y^*). \tag{11}$$

Let

$$\int_{\text{INT}} dV \equiv \int_{-H}^{0} dz \int_{-\infty}^{\infty} dx \int_{-\infty}^{\infty} dy, \qquad \int_{\text{ML}} dV \equiv \int_{0}^{1} dz \int_{-\infty}^{\infty} dx \int_{-\infty}^{\infty} dy$$

be the integrals over the interior of the ocean and the mixed layer, respectively. Assuming $A_{zz}A_y^* - A_{zz}^* A_y$ vanishes for $|y| \to \infty$ and using equation (8) gives the following results:

$$\frac{d}{dt}\int_{\text{INT}} |A_{zz}|^2 dV = \frac{i}{2}\int_{-\infty}^{\infty}\int_{-\infty}^{\infty} (A_{yz}^* A_y - A_{yz}A_y^*)|_{z=0^-}\, dxdy, \tag{12}$$

$$\frac{d}{dt}\int_{\text{ML}} \left|\frac{A_{zz}}{\epsilon^2}\right|^2 dV = -\frac{i}{2\epsilon^2}\int_{-\infty}^{\infty}\int_{-\infty}^{\infty} (A_{yz}^* A_y - A_{yz}A_y^*)|_{z=0^+}\, dxdy. \tag{13}$$

Equations (10),(12) and (13) may be combined to give

$$\frac{d}{dt}\int_{\text{INT}} |A_{zz}|^2 dV + \frac{d}{dt}\int_{\text{ML}} \left|\frac{A_{zz}}{\epsilon^2}\right|^2 dV = 0. \tag{14}$$

This is a statement of conservation of HKE in nondimensional form.

The quantity $F_E(y,t) \equiv \frac{i}{2}(A^*_{yz}A_y - A_{yz}A^*_y)|_{z=0^-}$ is the flux of HKE from the mixed layer to the interior of the ocean. Letting

$$\int_{V_d} dV \equiv \int_{-H}^{-d} dz \int_{-\infty}^{\infty} dx \int_{-\infty}^{\infty} dy,$$

similar arguments show that

$$\frac{d}{dt}\int_{V_d} |A_{zz}|^2 dV = \int_{-\infty}^{\infty}\int_{-\infty}^{\infty} F_E(y,t;d)dxdy, \tag{15}$$

where

$$F_E(y,t;d) \equiv \frac{i}{2}(A^*_{yz}A_y - A_{yz}A^*_y)|_{z=-d} \tag{16}$$

gives the flux of HKE from the region $z > -d$ to the region $z < -d$. Equation (12) is a special case of equation (15) with $F_E(y,t) \equiv F_E(y,t;0^-)$.

3.3 Integral Shear Relations and Shear Flux

In Section 3.4, it will shown that, to leading order in ϵ, A is independent of z in the mixed layer, and thus there is no shear in the mixed layer. For $z < 0$ the nondimensionalized buoyancy frequency is $N = 1$, so the vertical shear from equation (5) may be written in nondimensional form as $u_z^2 + v_z^2 = |A_{zzz}|^2$. Similar arguments to those leading to equations (6) and (11) give the evolution equation

$$\frac{\partial}{\partial t}|A_{zzz}|^2 = \frac{i}{2}\frac{\partial}{\partial y}(A_{zzz}A^*_{yz} - A^*_{zzz}A_{yz}) + \frac{i}{2}\frac{\partial}{\partial z}(A^*_{yzz}A_{yz} - A_{yzz}A^*_{yz}).$$

Assuming $A_{zzz}A^*_{yz} - A^*_{zzz}A_{yz}$ vanishes for $|y| \to \infty$,

$$\frac{d}{dt}\int_{V_d} |A_{zzz}|^2 dV = \int_{-\infty}^{\infty}\int_{-\infty}^{\infty} F_S(y,t;d)dxdy,$$

where

$$F_S(y,t;d) \equiv \frac{i}{2}(A^*_{yzz}A_{yz} - A_{yzz}A^*_{yz})|_{z=-d} \tag{17}$$

is the flux of vertical shear from the region $z > -d$ to the region $z < -d$.

3.4 Boundary Condition at Base of Mixed Layer

For $0 < z < 1$, equation (7) becomes

$$A_{zzt} + \frac{i}{2}\epsilon^2 A_{yy} + iyA_{zz} = 0.$$

Expanding $A(y,z,t) = A_0(y,z,t) + \epsilon^2 A_2(y,z,t) + \mathcal{O}(\epsilon^4)$,

$$A_{0zzt} + iyA_{0zz} = 0.$$

Integrating this subject to the boundary condition that A_z and thus A_{0z} vanishes at $z = 1$ gives

$$A_0 = e^{-iyt} \int_0^t g(y, t') e^{iyt'} dt'$$

for some function g. In particular, A_0 is independent of z. At $\mathcal{O}(\epsilon^2)$

$$A_{2zzt} + iyA_{2zz} + \frac{i}{2} A_{0yy} = 0, \tag{18}$$

which may be integrated subject to the boundary condition that A_{2z} vanishes at $z = 1$ to give

$$A_{2zt} + iyA_{2z} + \frac{i}{2} A_{0yy}(z - 1) = 0.$$

Evaluating at $z = 0^+$ and using

$$A_{yy} = A_{0yy} + \mathcal{O}(\epsilon^2), \qquad A_z = \epsilon^2 A_{2z} + \mathcal{O}(\epsilon^4), \qquad A_{zt} = \epsilon^2 A_{2zt} + \mathcal{O}(\epsilon^4)$$

implies that

$$A_{zt} + iyA_z - \frac{i\epsilon^2}{2} A_{yy} = \mathcal{O}(\epsilon^4) \qquad z = 0^+$$

Finally, applying (10) gives the boundary condition

$$A_{zt} + iyA_z - \frac{i}{2} A_{yy} = 0 \qquad z = 0^- \tag{19}$$

to leading order in ϵ.

3.5 Initial Condition

Suppose that in a short time compared with the NIO wave propagation time the passing storm causes near-inertial currents in the mixed layer with no horizontal structure. For simplicity, the initial velocity is assumed to be piecewise constant with depth. Thus the initial velocity profile (consistent with equation (4)) is taken to be

$$\begin{aligned} u &= 1 \qquad 0 < z < 1, \\ u &= -\frac{1}{H} \qquad -H < z < 0, \\ v &= 0 \qquad -H < z < 1. \end{aligned}$$

Integrating equation (9) with respect to z and using the boundary conditions (8) then gives at $t = 0$

$$A_z = \epsilon^2 (z - 1) \qquad 0 < z < 1 \tag{20}$$

$$A_z = -\frac{z + H}{H} \qquad -H < z < 0. \tag{21}$$

4 Solution for an Infinitely Deep Ocean

The total depth of the ocean is typically on the order of a hundred times the depth of the mixed layer; thus, the limit of infinite depth is considered. The initial condition is taken to be equation (21) with $H \to \infty$. The boundary condition for $z \to -\infty$ is taken to be $A_{zz} \to 0$, corresponding to the near-inertial velocities vanishing at infinite depth (see equation (3)). This limit does not invalidate the use of equation (1) which assumed hydrostatic balance and thus holds for the ocean having depth much smaller than the horizontal scales. The ocean still in reality has finite depth, but for depths just below the mixed layer it is *effectively* infinitely deep. Of course, this limit excludes the possibility of reflections off the bottom of the ocean which may be important (see, e.g., [9]); thus, the results should be viewed as what would happen in the absence of such reflections. Finally, the boundary condition for $z = 0^-$ given by equation (19) is used. For convenience, the problem to be solved for the semi-infinite domain $z < 0$ is summarized:

$$\begin{aligned} A_{zzt} + \frac{i}{2}A_{yy} + iyA_{zz} &= 0 && z < 0 \\ A_{zt} + iyA_z - \frac{i}{2}A_{yy} &= 0 && z = 0^- \\ A_{zz} &\to 0 && z \to -\infty \\ A_z &= -1 && t = 0. \end{aligned}$$

4.1 Solution by Laplace Transforms

Making the ansatz and definitions

$$A(y,z,t) = e^{-iyt}B(z,t), \qquad T \equiv \frac{t^3}{3}, \qquad \tilde{B}(z,T) \equiv B(z,t), \tag{22}$$

implies that

$$\tilde{B}_{zzT} - \frac{i}{2}\tilde{B} = 0 \qquad z < 0 \tag{23}$$

$$\tilde{B}_{zT} + \frac{i}{2}\tilde{B} = 0 \qquad z = 0^- \tag{24}$$

$$\tilde{B}_{zz} \to 0 \qquad z \to -\infty \tag{25}$$

$$\tilde{B}_z = -1 \qquad T = 0. \tag{26}$$

Laplace transforming equations (23)–(25) in time gives

$$b(z,p) \equiv \mathcal{L}[B(z,t)] = \int_0^\infty \tilde{B}(z,T)e^{-pT}dT \tag{27}$$

$$pb_{zz} - \tilde{B}_{zz}(z,0) - \frac{i}{2}b = 0 \qquad z < 0 \tag{28}$$

$$b_{zz} \to 0 \qquad z \to -\infty \tag{29}$$

$$pb_z - \tilde{B}_z(z,0) + \frac{i}{2}b = 0 \qquad z = 0^-. \tag{30}$$

$\tilde{B}_{zz}(z,0) = 0$ from equation (26); thus the solution to equation (28) satisfying the boundary condition (29) is

$$\begin{aligned} b(z,p) &= f(p)\exp\left(\frac{\alpha z}{\sqrt{p}}\right), \\ \alpha &\equiv \frac{1}{\sqrt{2}}\, e^{i\pi/4} = \frac{1}{2}(1+i). \end{aligned}$$

Using boundary condition (30) with $\tilde{B}_z(z,0) = -1$ from (26) determines $f(p)$, giving

$$b(z,p) = -\frac{1}{\alpha}\,\frac{1}{\sqrt{p}+\alpha}\,\exp\left(\frac{\alpha z}{\sqrt{p}}\right). \tag{31}$$

In principle, the problem is solved at this stage; inverting this Laplace transform gives $\tilde{B}(z,T)$, then $A(y,z,t)$ is obtained from equation (22). This can then be differentiated in order to determine various quantities of interest. In practice, it is more convenient to first differentiate with respect to z as appropriate, and then to invert the transform. This inversion may be done in three different ways: first, for $z = 0^-$ analytical expressions can be found, and these can be used to find analytical expressions for $0 < z < 1$; second, for other z values the inversion may be done numerically; and third, the asymptotic behavior can be determined by the method of steepest descents. But first, expressions for the flux of energy and shear in terms of the field $B(z,t)$ are given.

4.2 Flux of Energy and Shear

The energy and shear fluxes given in equations (16) and (17) may be related to the field B using equation (22), giving

$$\begin{aligned} F_E(t;d) &= \frac{i}{2}t^2(B_z^*B - B_zB^*)|_{z=-d} && (32)\\ &= t^2[\mathrm{Im}(B_z)\mathrm{Re}(B) - \mathrm{Re}(B_z)\mathrm{Im}(B)]|_{z=-d} && (33) \end{aligned}$$

$$\begin{aligned} F_S(t;d) &= \frac{i}{2}t^2(B_{zz}^*B_z - B_{zz}B_z^*)|_{z=-d} && (34)\\ &= t^2[\mathrm{Im}(B_{zz})\mathrm{Re}(B_z) - \mathrm{Re}(B_{zz})\mathrm{Im}(B_z)]|_{z=-d}. && (35) \end{aligned}$$

These fluxes are independent of y so the dependence on this variable is suppressed. Also, initially $A_{zz} = 0$ for $z < 0$. Integrating equation (15) with respect to time then gives

$$\int_{V_d} |A_{zz}|^2 dV = \int_{-\infty}^{\infty} dx \int_{-\infty}^{\infty} dy \int_0^t F_E(t;d)dt.$$

Thus

$$E(t;d) \equiv \int_0^t F_E(t;d)dt \tag{36}$$

is the total amount of HKE which has penetrated into the region $z < -d$. Calculating the initial amount of HKE in the mixed layer for the initial velocity profile shows that $E(t;d) \to 1$

corresponds to all energy originally in the mixed layer having reached depths below $z = -d$. The quantity

$$S(t;d) \equiv \int_0^t F_S(t;d)dt \tag{37}$$

is the integrated shear flux which has penetrated into the region $z < -d$. Note that the initial value of the shear for $z < 0$ and $z > 0$ is zero, but the total initial shear is infinite because of the discontinuity in the initial velocity profile at $z = 0$.

4.3 Analytical Solution for $z = 0^-$

For $z = 0^-$, inverse Laplace transforms are found in or deduced from a table in [1]. From equation (31),

$$b(0^-,p) = -\frac{1}{\alpha}\frac{1}{\sqrt{p}+\alpha},$$

and one obtains

$$\tilde{B}(0^-,T) = \mathcal{L}^{-1}[b(0^-,p)] = -\frac{1}{\alpha\sqrt{\pi T}} + e^{\alpha^2 T}\mathrm{erfc}(\alpha\sqrt{T}).$$

This is converted to the original time t using equation (22):

$$B(0^-,t) = -\frac{1}{\alpha}\left(\frac{3}{\pi t^3}\right)^{1/2} + e^{\alpha^2 t^3/3}\mathrm{erfc}(\frac{\alpha}{\sqrt{3}}\,t^{3/2}). \tag{38}$$

Differentiating equation (31) with respect to z and evaluating at $z = 0^-$ gives

$$\begin{aligned}
b_z(0^-,p) &= -\frac{1}{p+\alpha\sqrt{p}} \qquad \Rightarrow B_z(0^-,t) = -e^{\alpha^2 t^3/3}\mathrm{erfc}(\frac{\alpha}{\sqrt{3}}\,t^{3/2}),\\
b_{zz}(0^-,t) &= -\frac{\alpha}{p(\sqrt{p}+\alpha)} \;\Rightarrow B_{zz}(0^-,t) = e^{\alpha^2 t^3/3}\mathrm{erfc}(\frac{\alpha}{\sqrt{3}}\,t^{3/2}) - 1, \qquad (39)\\
b_{zzz}(0^-,p) &= -\frac{\alpha^2}{p(p+\alpha\sqrt{p})}\\
\Rightarrow \qquad & B_{zzz}(0^-,t) = 1 - e^{\alpha^2 t^3/3}\mathrm{erfc}(\frac{\alpha}{\sqrt{3}}\,t^{3/2}) - 2\alpha\left(\frac{t^3}{3\pi}\right)^{1/2}. \qquad (40)
\end{aligned}$$

The solid lines (labelled d = 0) in Figure 1 show the quantities F_E, F_S, E, and S calculated using the results of this section. F_E peaks at the nondimensionalized time $t \approx 0.62$; for the typical values quoted in Section 3.1, this corresponds to about a week after the storm. From Figure 1(b) and using the fact that whatever energy flows through $z = 0^-$ must have initally been in the mixed layer, we see that by $t = 1$ (approximately 11.5 days after the storm) nearly half of the energy associated with horizontal NIO currents caused by the storm has left the mixed layer. By $t = 2$ (approximately 23 days after the storm) 82% has left, while by $t = 3$ (just over a month after the storm) 93% has left. Although this simplified model cannot be expected to capture the full complexity of a real storm over the ocean, it does give reasonable estimates for the time scale for which the decay of NIO energy occurs: [8] found that the mixed layer inertial energy was reduced to background levels by 21 days after the storm. Both the shear flux F_S and the integrated shear S increase monotonically with time, an artifact of the initial velocity profile being discontinuous at $z = 0$.

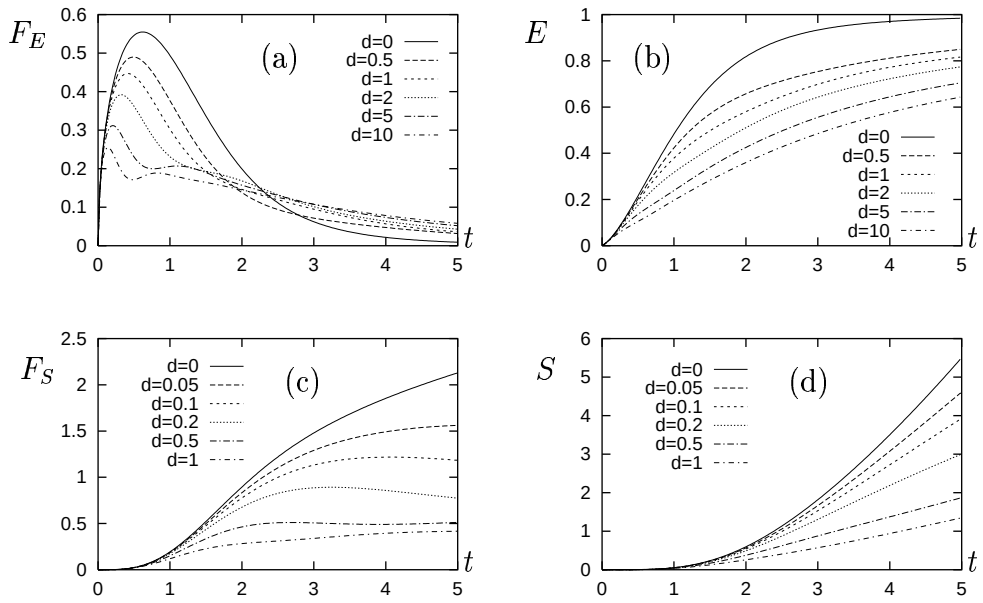

Figure 1: (a) $F_E(t;d)$, (b) $E(t;d)$, (c) $F_S(t;d)$, and (d) $S(t;d)$ for different distances d below the base of the mixed layer. These show instantaneous and integrated fluxes of energy and shear; see the text for precise definitions. The solid lines (labelled d = 0) give results at $z = 0^-$.

4.4 Analytical Solution for the Mixed Layer

Expanding $B(z,t) = B_0(z,t) + \epsilon^2 B_2(z,t) + \mathcal{O}(\epsilon^4)$ for the interval $0 < z < 1$,

$$\begin{aligned} A_0(y,z,t) &= e^{-iyt} B_0(z,t) \equiv e^{-iyt} \tilde{B}_0(z,T), \\ A_2(y,z,t) &= e^{-iyt} B_2(z,t) \equiv e^{-iyt} \tilde{B}_2(z,T), \end{aligned}$$

where $T = t^3/3$ as before. Equation (18) then implies that

$$\tilde{B}_{2zzT} - \frac{i}{2}\tilde{B}_0 = 0 \qquad 0 < z < 1.$$

This is Laplace transformed to give

$$p b_{2zz} - \tilde{B}_{2zz}(z,0) - \frac{i}{2} b_0 = 0, \tag{41}$$

where $b_2 = \mathcal{L}[\tilde{B}_2]$ and $b_0 = \mathcal{L}[\tilde{B}_0]$. The initial condition within the mixed layer is $A_{zz} = \epsilon^2$, so $A_{2zz} = 1$ at $t = 0$; thus $\tilde{B}_{2zz}(z,0) = 1$. Now, A is continuous across $z = 0$, and $A = A_0$ to leading order in ϵ. This implies that $\tilde{B}_0(0^+,T) = \tilde{B}(0^-,T)$ to leading order in ϵ. Also, A_0 and hence $\tilde{B}_0$ are independent of z. Laplace transforming, we conclude that the value of b_0 for $0 < z < 1$ is equal to $b(0^-,p)$. Using all of this and equation (31) evaluated at $z = 0^-$ in equation (41),

$$b_{2zz} = \frac{1}{p} - \frac{i}{2\alpha}\frac{1}{\sqrt{p}+\alpha} \Rightarrow B_{2zz} = e^{\alpha^2 t^3/3}\mathrm{erfc}(\frac{\alpha}{\sqrt{3}}t^{3/2})$$

Thus,

$$A_{2zz}(y,t) = e^{-iyt} e^{\alpha^2 t^3/3} \mathrm{erfc}(\frac{\alpha}{\sqrt{3}}\, t^{3/2}). \tag{42}$$

The local HKE is, to leading order, $|A_{2zz}|^2 = |A_{zz}/\epsilon^2|^2$; the total HKE contained within the mixed layer is

$$\int_{\mathrm{ML}} \left| \frac{A_{zz}}{\epsilon^2} \right|^2 dV = \int_{\mathrm{ML}} |A_{2zz}|^2 dV.$$

Using $\alpha^2 = i/2$, the amount of HKE per unit volume within the mixed layer is

$$\epsilon_{\mathrm{ML}} \equiv \left| \mathrm{erfc}(\frac{\alpha}{\sqrt{3}}\, t^{3/2}) \right|^2. \tag{43}$$

From [1],

$$\begin{aligned} e^{\alpha^2 t^3/3} \mathrm{erfc}(\frac{\alpha}{\sqrt{3}}\, t^{3/2}) &\sim \sqrt{\frac{3}{\pi}}\, \frac{1}{\alpha t^{3/2}} \qquad t \to \infty \\ \Rightarrow \quad \epsilon_{\mathrm{ML}} &\sim \frac{6}{\pi t^3} \qquad t \to \infty. \end{aligned}$$

This asymptotic relationship is confirmed in Figure 2. Since A_{2zz} is independent of z, to leading order in ϵ the shear within the mixed layer is zero.

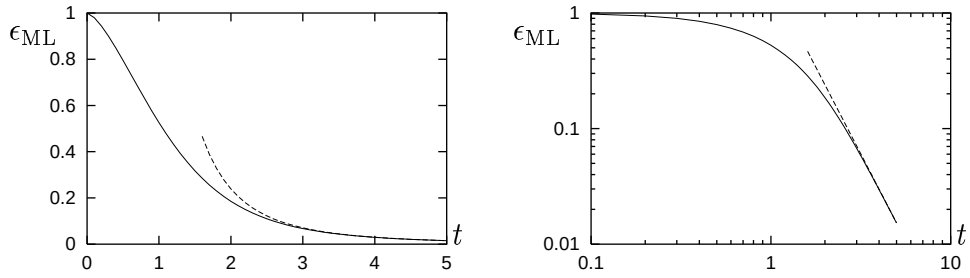

Figure 2: ϵ_{ML} gives the HKE per unit volume in the mixed layer. The solid line shows the exact result and the dashed line shows the asymptotic result, shown both for linear and logarithmic axes.

4.5 Solution for Other Depths

A tractable analytical form for the inverse Laplace transform of equation (31) for $z \neq 0$ could not be found; however, it may be inverted numerically as described in this section. The inverse Laplace transform is given by

$$\tilde{B}(z,T) = -\frac{1}{2\pi\alpha i} \int_{\mathcal{B}} \frac{\exp(\frac{\alpha z}{\sqrt{p}} + pT)}{\sqrt{p} + \alpha} dp,$$

where $\mathcal{B}$ is the Bromwich contour. Here the branch cut for the square root is taken to be along the negative real axis, and the principal branch is chosen. The integrand does not have

any poles on this sheet of the Riemann surface. Such a pole would satisfy $\sqrt{p}+\alpha=0$, and would be given by $p_p=\alpha^2=e^{i\pi/2}/2$; however, $\sqrt{p_p}+\alpha=\sqrt{2}e^{i\pi/4}\neq 0$ and thus there is no pole. It is useful to make the change of variables (valid for $z\neq 0$ and $T\neq 0$)

$$p=\left(-\frac{z}{T}\right)^{2/3}w, \qquad \xi\equiv(z^2T)^{1/3}, \qquad \eta\equiv\left(-\frac{z}{T}\right)^{1/3}. \tag{44}$$

Then,

$$\tilde{B}(z,T) = -\frac{\eta^2}{2\pi\alpha i}\int_{\mathcal{B}}\frac{\exp[\xi(-\frac{\alpha}{\sqrt{w}}+w)]}{\eta\sqrt{w}+\alpha}dw \tag{45}$$

$$\equiv -\frac{\eta^2}{2\pi\alpha i}\int_{\mathcal{B}} g(w;\xi,\eta)dw. \tag{46}$$

Defining the contour $\mathcal{C}$ as in Figure 3 and using the facts that the contributions from $\mathcal{C}_1$ and $\mathcal{C}_2$ vanish and that there are no poles,

$$\int_{\mathcal{C}} g(w;\xi,\eta)dw=\left\{\int_{\mathcal{B}}+\int_{\mathrm{AB}}+\int_{\mathrm{BC}}+\int_{\mathrm{CD}}\right\}g(w;\xi,\eta)dw=0.$$

For the path AB, $w=re^{i\pi}$ and

$$I_{\mathrm{AB}}\equiv\int_{\mathrm{AB}}g(w;\xi,\eta)=\int_1^\infty\frac{e^{-r\xi}e^{i\alpha\xi/\sqrt{r}}}{\eta i\sqrt{r}+\alpha}dr.$$

For the path BC, $w=e^{i\theta}$ and

$$I_{\mathrm{BC}}\equiv\int_{\mathrm{BC}}g(w;\xi,\eta)=-i\int_{-\pi}^{\pi}\frac{\exp[\xi(-\alpha e^{-i\theta/2}+e^{i\theta})]e^{i\theta}}{\eta e^{i\theta/2}+\alpha}d\theta.$$

Finally, for the path CD, $w=re^{-i\pi}$ and

$$I_{\mathrm{CD}}\equiv\int_{\mathrm{CD}}g(w;\xi,\eta)=-\int_1^\infty\frac{e^{-r\xi}e^{-i\alpha\xi/\sqrt{r}}}{-\eta i\sqrt{r}+\alpha}dr.$$

Specifying z and T fixes ξ and η. The integrals I_{AB}, I_{BC}, and I_{CD} are well-behaved and can be calculated numerically. Then

$$\tilde{B}(z,T)=\frac{\eta^2}{2\pi\alpha i}(I_{\mathrm{AB}}+I_{\mathrm{BC}}+I_{\mathrm{CD}}).$$

Differentiating (31) with respect to z,

$$b_z(z,p) = -\frac{1}{p+\alpha\sqrt{p}}\,\exp\left(\frac{\alpha z}{\sqrt{p}}\right),$$

$$b_{zz}(z,p) = -\frac{\alpha}{p(\sqrt{p}+\alpha)}\,\exp\left(\frac{\alpha z}{\sqrt{p}}\right),$$

$$b_{zzz}(z,p) = -\frac{\alpha^2}{p(p+\alpha\sqrt{p})}\,\exp\left(\frac{\alpha z}{\sqrt{p}}\right).$$

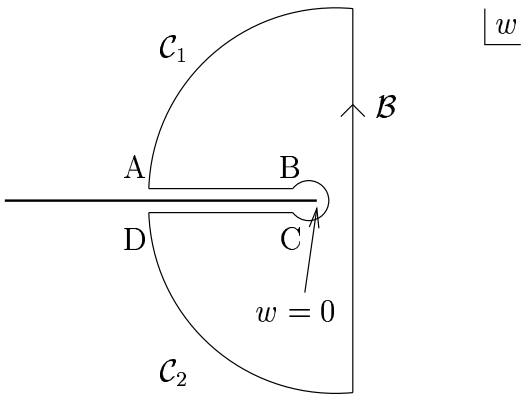

Figure 3: Contour used to determine inverse Laplace transformations. Here A=$(-\infty, 0^+)$, B=$(-1, 0^+)$, C=$(-1, 0^-)$, and D=$(-\infty, 0^-)$.

Using the contour in Figure 3, we find

$$\begin{aligned}
\tilde{B}_z(z,T) &= \frac{\eta^2}{2\pi i}(I^{(1)}_{\rm AB} + I^{(1)}_{\rm BC} + I^{(1)}_{\rm CD}),\\
\tilde{B}_{zz}(z,T) &= \frac{\alpha\eta^2}{2\pi i}(I^{(2)}_{\rm AB} + I^{(2)}_{\rm BC} + I^{(2)}_{\rm CD}),\\
\tilde{B}_{zzz}(z,T) &= \frac{\alpha^2\eta^2}{2\pi i}(I^{(3)}_{\rm AB} + I^{(3)}_{\rm BC} + I^{(3)}_{\rm CD}),
\end{aligned}$$

where

$$I^{(1)}_{\rm AB} = \int_1^\infty \frac{e^{-r\xi}e^{i\alpha\xi/\sqrt{r}}}{-\eta^2 r + \eta\alpha i\sqrt{r}}dr, \qquad I^{(1)}_{\rm BC} = -i\int_{-\pi}^{\pi} \frac{\exp[\xi(-\alpha e^{-i\theta/2} + e^{i\theta})]}{\eta^2 + \eta\alpha e^{-i\theta/2}}d\theta,$$

$$I^{(1)}_{\rm CD} = \int_1^\infty \frac{e^{-r\xi}e^{-i\alpha\xi/\sqrt{r}}}{\eta^2 r + \eta\alpha i\sqrt{r}}dr, \qquad I^{(2)}_{\rm AB} = -\int_1^\infty \frac{e^{-r\xi}e^{i\alpha\xi/\sqrt{r}}}{\eta^3 i r^{3/2} + \eta^2\alpha r}dr,$$

$$I^{(2)}_{\rm BC} = -i\int_{-\pi}^{\pi} \frac{\exp[\xi(-\alpha e^{-i\theta/2} + e^{i\theta})]}{\eta^3 e^{i\theta/2} + \eta^2\alpha}d\theta, \qquad I^{(2)}_{\rm CD} = \int_1^\infty \frac{e^{-r\xi}e^{-i\alpha\xi/\sqrt{r}}}{-\eta^3 i r^{3/2} + \eta^2\alpha r}dr,$$

$$I^{(3)}_{\rm AB} = \int_1^\infty \frac{e^{-r\xi}e^{i\alpha\xi/\sqrt{r}}}{\eta^4 r^2 - \eta^3\alpha i r^{3/2}}dr, \qquad I^{(3)}_{\rm BC} = -i\int_{-\pi}^{\pi} \frac{\exp[\xi(-\alpha e^{-i\theta/2} + e^{i\theta})]}{\eta^4 e^{i\theta} + \alpha\eta^3 e^{i\theta/2}}d\theta,$$

$$I^{(3)}_{\rm CD} = -\int_1^\infty \frac{e^{-r\xi}e^{-i\alpha\xi/\sqrt{r}}}{\eta^4 r^2 + \alpha\eta^3 i r^{3/2}}dr.$$

All of these integrals are well-behaved and can be calculated numerically.

4.6 Results

4.6.1 Fluxes and Integrated Fluxes

The quantities $F_E(t;d), F_S(t;d), E(t;d)$, and $S(t;d)$ may now be calculated and results are shown in Figure 1. From Figure 1(b), as noted in Section 4.3, by $t = 1$ nearly half of the total

horizontal near inertial energy has left the mixed layer; only about 38% of the total energy has penetrated below $z = -1$. By $t = 2$, 82% of the total energy has left the mixed layer, but only 58% of the total energy has penetrated below $z = -1$. Thus, at $t = 2$ (using the typical values quoted in Section 3.1, about 23 days after the storm) nearly a quarter of the total energy is contained in the distance H_{mix} immediately beneath the mixed layer. Figure 1(d) demonstrates that the shear tends to be localized just below the base of the mixed layer. For example, by $t = 5$ the integrated shear flux which has entered the mixed layer is, in nondimensional units, about 5.5. The integrated shear flux which has penetrated below $z = -0.05$ is 4.6, and the integrated shear flux which has penetrated below $z = -1$ is 1.35.

4.6.2 Vertical Profiles

Using the expressions from Section 4.5 and equation (22) it is now also possible to calculate vertical profiles of physically relevant quantities. Figure 4(a,b) shows the vertical dependence of the HKE, $u^2 + v^2 = |A_{zz}|^2$, and the vertical shear, $u_z^2 + v_z^2 = |A_{zzz}|^2$, at different times for $y = 0$. For both quantities, as time increases the instantaneous distribution becomes more sharply peaked near the base of the mixed layer. The maximum value of $u_z^2 + v_z^2$ increases without bound as time increases, but the maximum value of u^2+v^2 remains bounded (asymptotically approaching unity) because of energy conservation. Figure 4(c,d) shows the vertical dependence of the fluxes F_E and F_S.

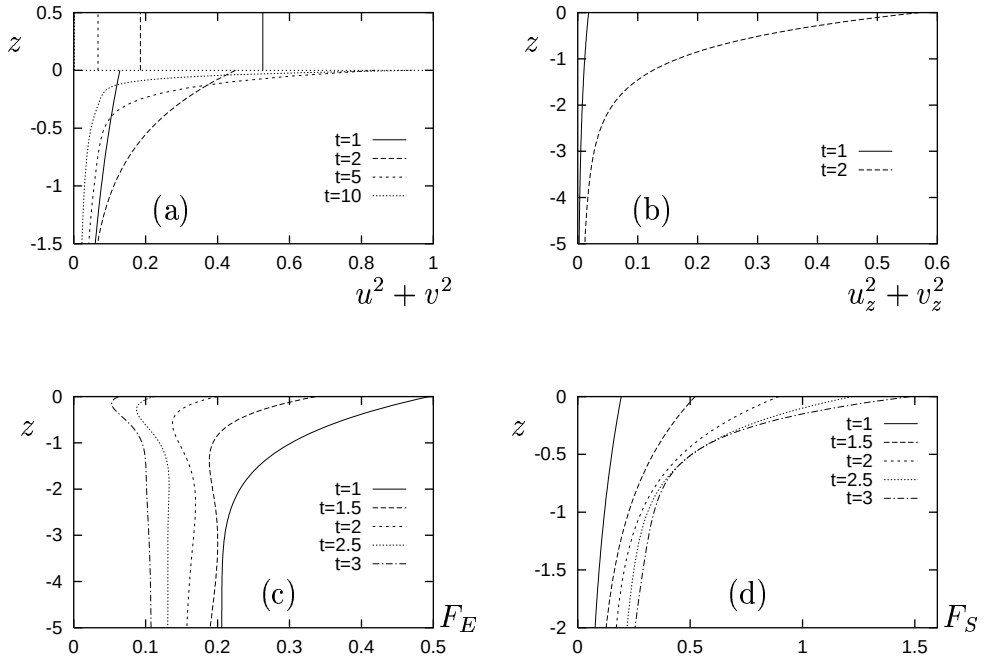

Figure 4: Vertical profiles of (a) $u^2 + v^2$ and (b) $u_z^2 + v_z^2$ at $y = 0$ for different times showing the decay of energy from the mixed layer ($0 < z < 1$) and resultant behavior in the interior ($z < 0$). Note that $u_z^2 + v_z^2 = 0$ in the mixed layer to leading order in ϵ. Also, vertical profiles of (c) $F_E(t, |z|)$, and (d) $F_S(t, |z|)$ for different times. Note the different vertical scales.

4.6.3 Back-Rotated Velocity and Shear

Finally, consider the back-rotated velocity $A_{zz} = e^{if_0 t}(u + iv)$. This filters out the purely intertial motion at frequency f_0. Similarly, the back-rotated shear is defined to be $A_{zzz} = e^{if_0 t}(u_z + iv_z)$. The amplitudes of the back-rotated velocity and shear at different depths are shown as time series in Figure 5. At a given depth, the magnitude of the back-rotated velocity reaches a peak value shortly after the storm, then decays away, while the magnitude of the back-rotated shear increases monotonically with time. Note that Figure 4, may also be interpreted in terms of the back-rotated velocity and shear.

Back-rotated velocity and shear may be represented by hodographs which respectively show the vectors $(\mathrm{Re}(A_{zz}), \mathrm{Im}(A_{zz}))$ and $(\mathrm{Re}(A_{zzz}), \mathrm{Im}(A_{zzz}))$ as curves parametrized by time. For $f_0 > 0$, if these curves are traced out in a clockwise (counterclockwise) fashion, the corresponding motion has frequency larger (smaller) than f_0. Figure 6 shows the back-rotated velocity and shear at $y = 0, z = -1$. The hodographs for both quantities start at the origin and are traced out in a clockwise fashion. The back-rotated velocity starts out in the third quadrant, reaches a peak in magnitude in the second quadrant, then decays in magnitude spiralling back to the origin. The back-rotated shear also starts out in the third quadrant, and monotonically increases in magnitude while spiralling outward. Note that the lines labelled $z = -1$ in Figure 5 give the radii of these hodographs as functions of time. The depth dependence of the back-rotated velocity is seen by comparing Figure 6 with Figure 7(a), where both have $y = 0$ and thus the same value of the Coriolis parameter. Qualitatively the results are the same, but closer to the mixed layer the direction change of the back-rotated velocity becomes slower, meaning that the frequency is closer to f_0. An idea of the latitudinal dependence is seen by comparing Figure 6 with Figure 7(b,c). At $y = 1$ the hodograph is traced out in a clockwise fashion as for $y = 0$, but at $y = -2$ it is traced out in a counterclockwise fashion.

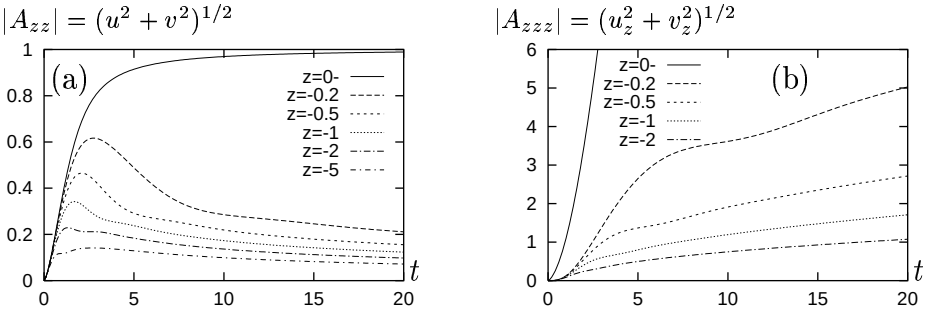

Figure 5: Time series for $|A_{zz}|$ and $|A_{zzz}|$ at different fixed z values.

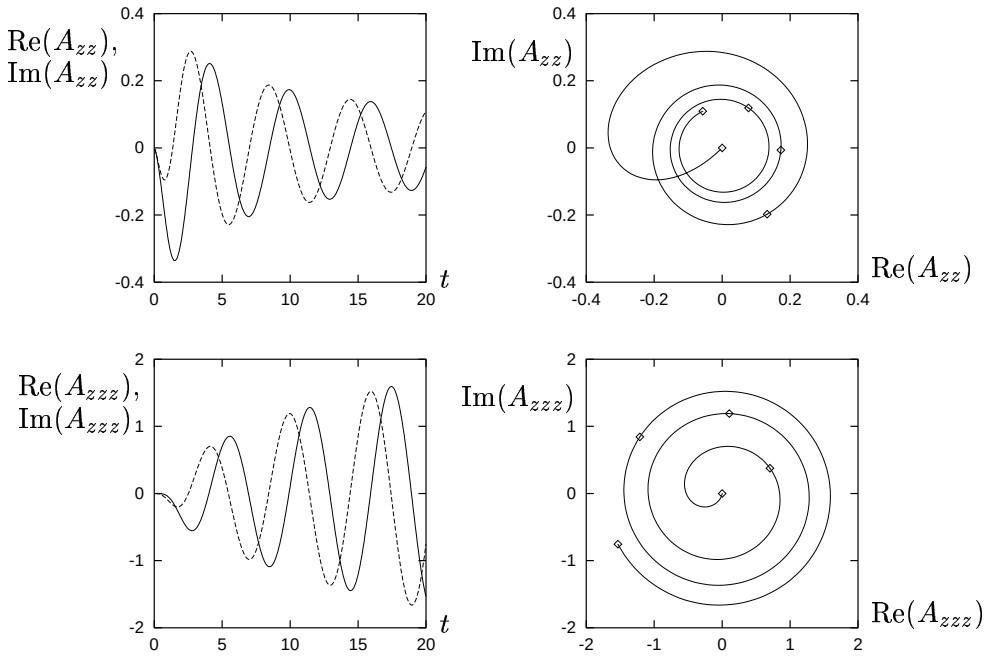

Figure 6: Back-rotated velocity and shear at $z = -1, y = 0$. In these and the time series in Figure 7, the solid and dashed lines show real and imaginary parts, respectively. The diamonds are drawn at $t = 0, 5, 10, 15, 20$.

4.7 Asymptotic Behavior

Making the change of variables (44), the inverse Laplace transforms of b, b_z, b_{zz}, and b_{zzz} can be written in the form

$$\begin{aligned} I(\xi) &= \int_{\mathcal{B}} f(w,\eta) e^{\xi h(w)} dw, \\ h(w) &\equiv -\frac{\alpha}{\sqrt{w}} + w. \end{aligned}$$

The asymptotic behavior of this in the limit of large ξ with η fixed can be determined by the method of steepest descents. This involves determining the saddle points of $h(w)$ (i.e., points satisfying $h'(w) = 0$) and deforming the contour $\mathcal{B}$ so as to pass through each saddle point along a path of constant $\mathrm{Im}(h(w))$ such that $\mathrm{Re}(h(w))$ has a local maximum at each saddle point. Supposing that there is a simple saddle ($h''(w_0) \neq 0$) at $w = w_0$,

$$I(\xi) \sim \frac{\sqrt{2\pi} f(w_0) e^{\xi h(w_0)} e^{i\gamma}}{|\xi h''(w_0)|^{1/2}}. \tag{47}$$

Here γ is the angle relative to the positive real axis at which the path satisfying the above conditions passes through the saddle. Letting $h''(w_0) = ae^{i\sigma}$, $\gamma = -\sigma/2 + \pi/2$ or $\gamma = -\sigma/2 + 3\pi/2$; the appropriate choice is determined by making sure that $h(w)$ only has local maxima at the saddle points and no where else along the deformed contour.

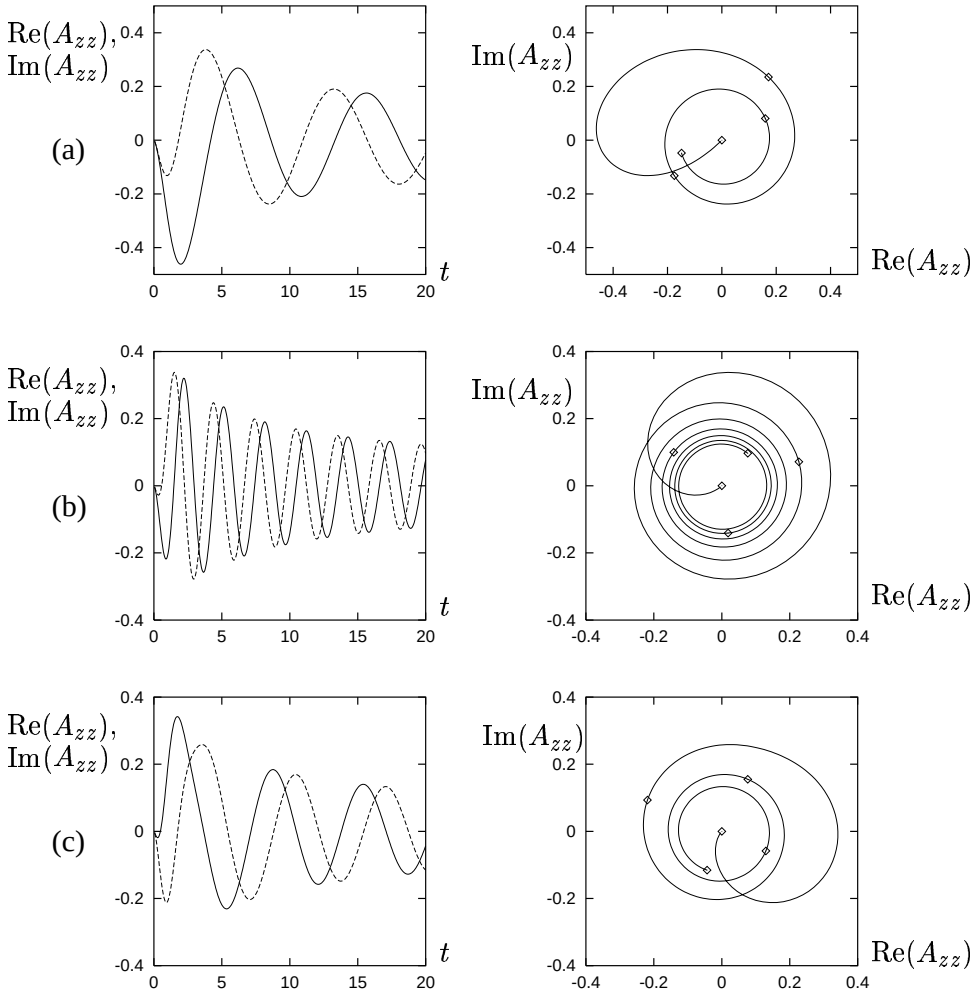

Figure 7: Back-rotated velocity for (a) $z = -0.5, y = 0$, (b) $z = -1, y = 1$, and (c) $z = -1, y = -2$. The conventions of Figure 6 are also used for this Figure.

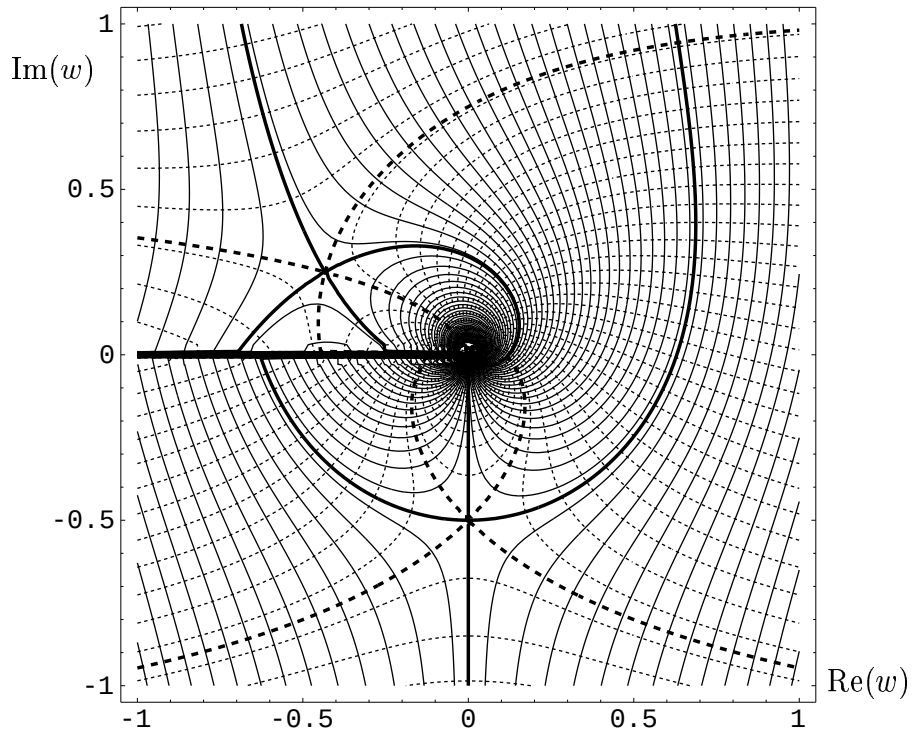

Figure 8: Contours of constant $\mathrm{Re}(h(w))$ (solid lines) and $\mathrm{Im}(h(w))$ (dashed lines) in the complex w plane. The thick lines are the contours passing through the saddle points. The branch cut is clearly seen along the negative real axis. In the method of steepest descents, the Bromwich contour is deformed to pass through $w_1 = e^{-i\pi/2}/2 = -i/2$ with angle $\gamma = \pi/4$, to the right of the origin avoiding the branch cut, and through $w_2 = e^{i\pi 5/6}/2$ with angle $\gamma = 11\pi/12$.

Taking the branch cut for the square root along the negative real axis, for this problem, there are saddles at

$$w_1 = \frac{1}{2}e^{-i\pi/2}, \qquad w_2 = \frac{1}{2}e^{i\pi 5/6}$$

with

$$\begin{aligned} h(w_1) &= -\frac{3}{2}i, \qquad h(w_2) = -\frac{3\sqrt{3}}{4} + \frac{3}{4}i \\ h''(w_1) &= 3i, \qquad h''(w_2) = 3e^{-i\pi 5/6}. \end{aligned}$$

Figure 8 shows the contours of constant real and imaginary parts of $h(w)$. The deformed contour is taken to pass through both of these saddles, and passes to the right of the origin in order to avoid the branch cut. Since $h(w_1)$ is purely imaginary and $h(w_2)$ has negative real part, it is immediately seen that the contribution from w_2 will be exponentially small compared with the contribution from w_1 in the limit $\xi \to \infty$. Using $\gamma = \pi/4$ for the passage

through w_1, in the limit $\xi \to \infty$ with η fixed

$$I(\xi) \sim \sqrt{\frac{2\pi}{3}}\, \xi^{-1/2}\, f(w_1)\, e^{i(-3\xi/2+\pi/4)}. \tag{48}$$

This implies that

$$\begin{aligned}
B &\sim \frac{\eta^2(1+i\eta)}{\pi(1+\eta^2)}\sqrt{\frac{2\pi}{3}}\, \xi^{-1/2}\, e^{i(-3\xi/2+\pi/4)},\\
B_z &\sim \frac{\eta(i-\eta)}{\pi(1+\eta^2)}\sqrt{\frac{2\pi}{3}}\, \xi^{-1/2}\, e^{i(-3\xi/2+\pi/4)},\\
B_{zz} &\sim -\frac{1+i\eta}{\pi(1+\eta^2)}\sqrt{\frac{2\pi}{3}}\, \xi^{-1/2}\, e^{i(-3\xi/2+\pi/4)},\\
B_{zzz} &\sim \frac{\eta-i}{\eta\pi(1+\eta^2)}\sqrt{\frac{2\pi}{3}}\, \xi^{-1/2}\, e^{i(-3\xi/2+\pi/4)}.
\end{aligned}$$

Now, using $\xi = \eta^2 T = \eta^2 t^3/3$ and taking the constant η to be η_0, along the "rays" $z = -\eta_0^3 t^3/3$,

$$\begin{aligned}
u^2+v^2 &= |A_{zz}|^2 = |B_{zz}|^2 \sim \frac{2}{(1+\eta_0^2)\pi\eta_0^2 t^3},\\
u_z^2+v_z^2 &= |A_{zzz}|^2 = |B_{zzz}|^2 \sim \frac{2}{\pi\eta_0^4(1+\eta_0^2)t^3},\\
F_E &= t^2[\mathrm{Im}(B_z)\mathrm{Re}(B) - \mathrm{Re}(B_z)\mathrm{Im}(B)]|_{z=-\eta_0^3 t^3/3} \sim \frac{2\eta_0}{\pi(1+\eta_0^2)t},\\
F_S &= t^2[\mathrm{Im}(B_{zz})\mathrm{Re}(B_z) - \mathrm{Re}(B_{zz})\mathrm{Im}(B_z)]|_{z=-\eta_0^3 t^3/3} \sim \frac{2}{\pi\eta_0(1+\eta_0^2)t}.
\end{aligned}$$

These asymptotic relationships are confirmed in Figure 9. A more useful way to represent the asymptotic results is to write η_0 in terms of z and t and then draw contour plots of quantities of physical interest in the (z,t) plane; this is shown in Figure 10. Note that ξ is large for sufficiently large z and/or t. For example, this shows that in the asymptotic limit for constant z, as time increases, u^2+v^2 and F_E decrease, while $u_z^2+v_z^2$ and F_S increase.

5 Conclusion

In this paper, a simplified model has been developed and studied for the decay of near-inertial currents excited in the mixed layer by a passing storm. This decay occurs due to the radiation of downward propagating NIOs into the interior of the ocean. The main assumptions of the model are that the background flow does not vary in the longitudinal direction and has no associated vorticity, the ocean has a simple (piecewise constant) buoyancy frequency profile, and the storm has moved very quickly over the ocean causing a horizontally uniform near-inertial current concentrated in the mixed layer. The β effect is included in the analysis. Because the depth of the mixed layer is much smaller than the total depth of the ocean, the

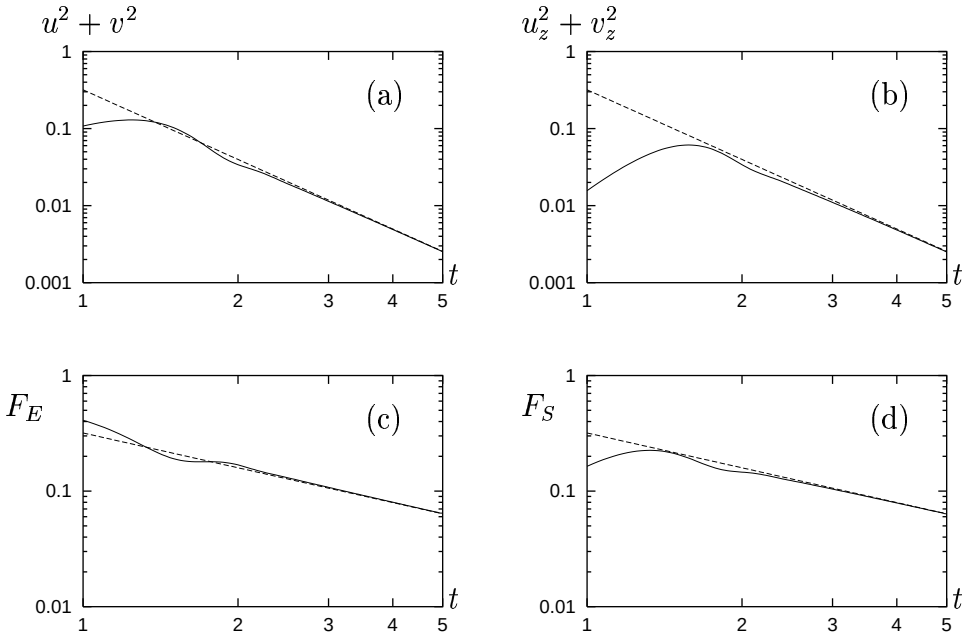

Figure 9: Comparison of numerically calculated (solid lines) and asymptotic (dashed lines) results along the ray $z = -t^3/3$, i.e., $\eta_0 = 1$. (a) $u^2 + v^2$, (b) $u_z^2 + v_z^2$, (c) F_E, (d) F_S.

problem is formulated in the limit of an effectively infinitely deep ocean; the resultant initial value problem is solved by Laplace transforms. Analytical and numerical results are given for quantities of physical interest including horizontal kinetic energy, vertical shear, energy and shear flux, and back-rotated velocity and shear. Also, asymptotic behavior is determined by the method of steepest descents.

Although this simplified model cannot be expected to capture the full complexity of the aftermath of a storm passing the ocean, it does capture much of the observed behavior. Most importantly, the decay of mixed layer energy is found to occur on the appropriate timescale (approximately twenty days). It would be interesting to compare the results obtained for this simplified model with observations and numerical simulations. Also, from both a computational and a more philosophical perspective, it would be interesting to compare this method of solution with the standard approach of projecting onto normal modes (e.g., [2, 3]). In the latter, the decay must be viewed as a complicated interference between normal modes, while in the method presented in this paper it is more naturally viewed as a radiation problem. Extensions to a more realistic ocean and storm would involve including a more realistic buoyancy frequency profile (for example, the profile used by [10]), considering the effect of different initial velocities (including both horizontal and vertical structure), and considering the effect of background flow. The study of all of these could use the same formalism of [18] and an approach similar to that presented here.

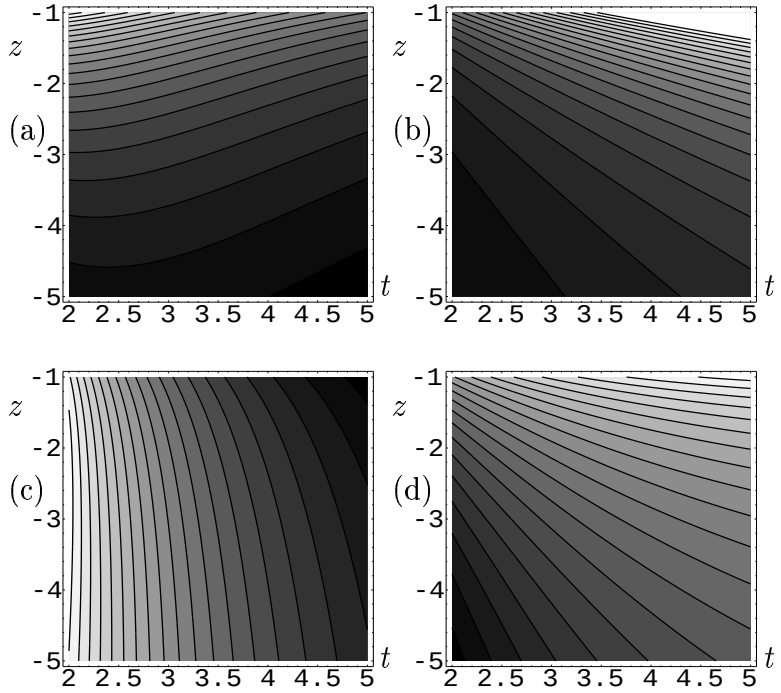

Figure 10: Contour plots of the asymptotic results for (a) $u^2 + v^2$, (b) $u_z^2 + v_z^2$, (c) F_E, (d) F_S. Darker shading corresponds to smaller values.

Acknowledgments

I would like to thank Bill Young and Stefan Llewellyn Smith for providing so much useful guidance on this project. I enjoyed learning some oceanography, and it was nice to be reminded that linear problems can be quite interesting and rich. Thanks also to Neil Balmforth for directing a great program, and to all the other fellows and staff for an enjoyable summer. Finally, thanks to my wife Allison for making our honeymoon in Woods Hole so wonderful.

References

[1] Abramowitz, M. and Stegun, I. A. (1972) Handbook of Mathematical Functions, Wiley Interscience Publications, 1046 pp.

[2] Balmforth, N. J., Llewellyn Smith, S. G. and Young, W. R. (1998) Enhanced dispersion of near-inertial waves in an idealized geostrophic flow. *J. Mar. Res.*, 56:1–40.

[3] Balmforth, N. J. and Young, W. R. (1999) Radiative damping of near-inertial oscillations in the mixed layer, preprint.

[4] Cushman-Roisin, B. (1994) Introduction to Geophysical Fluid Dynamics, Prentice Hall, 320 pp.

[5] D'Asaro, E. A. (1985) The energy flux from the wind to near-inertial motions in the surface mixed layer. *J. Phys. Oceanogr.*, 15:1043–1059.

[6] D'Asaro, E. A. (1989) The decay of wind-forced mixed layer inertial oscillations due to the β effect. *J. Geophys. Res.*, 94:2045–2056.

[7] D'Asaro, E. A. (1995) Upper-ocean inertial currents forced by a strong storm. Part II: Modelling. *J. Phys. Oceanogr.*, 25:2937–2952.

[8] D'Asaro, E. A., Eriksen, C. C., Levine, M. D., Niiler, P., Paulson, C. A., and van Meurs, P. (1995) Upper-ocean inertial currents forced by a strong storm. Part I: Data and comparisons with linear theory. *J. Phys. Oceanogr.*, 25:2909–2936.

[9] Garrett, C. (1999) What is the "near-inertial" band and why is it different?, preprint.

[10] Gill, A. E. (1984) On the behavior of internal waves in the wakes of storms. *J. Phys. Oceanogr.*, 14:1129–1151.

[11] Hebert, D. and Moum, J. N. (1993) Decay of a near-inertial wave. *J. Phys. Oceanogr.*, 24:2334–2351.

[12] Henyey, F. S., Wright, J. A., and Flatté, S. M. (1986) Energy and action flow through the internal wave field: an eikonal approach. *J. Geophys. Res.*, 91(C7):8487–8495.

[13] Levine, M. D. and Zervakis, V. (1995) Near-inertial wave propagation into the pycnocline during ocean storms: observations and model comparison. *J. Phys. Oceanogr.*, 25:2890–2908.

[14] Pollard, R. T. and Millard, R. C. Jr. (1970) Comparison between observed and simulated wind-generated inertial oscillations. *Deep-Sea Res.*, 17:813–821.

[15] Qi, H., De Szoeke, R. A., Paulson, C. A., and Eriksen, C. C. (1995) The structure of near-inertial waves during ocean storms. *J. Phys. Oceanogr.*, 25:2853–2871.

[16] van Meurs, P. (1998) Interactions between near-inertial mixed layer currents and the mesoscale: the importance of spatial variabilities in the vorticity field. *J. Phys. Oceanogr.*, 28:1363–1388.

[17] Webster, F. (1968) Observation of inertial-period motions in the deep sea. *Rev. Geophys.*, 6:473–490.

[18] Young, W. R. and Ben Jelloul, M. (1997) Propagation of near-inertial oscillations through a geostrophic flow. *J. Mar. Res.*, 55:735–766.

[19] Zervakis, V. and Levine, M. D. (1995) Near-inertial energy propagation from the mixed layer: theoretical considerations. *J. Phys. Oceanogr.*, 25:2872–2889.